Journal of Membrane Science 342 (2009) 263–268

Contents lists available at ScienceDirect

Journal of Membrane Science

journal homepage: www.elsevier.com/locate/memsci

Controlling biofilm growth using reactive ceramic ultrafiltration membranes

Shannon Ciston[a], Richard M. Lueptow[b], Kimberly A. Gray[c,a,*]

[a] Department of Chemical and Biological Engineering, Northwestern University, 2145 Sheridan Road, Evanston, IL 60208, USA
[b] Department of Mechanical Engineering, Northwestern University, 2145 Sheridan Road, Evanston, IL 60208, USA
[c] Department of Civil and Environmental Engineering, Northwestern University, 2145 Sheridan Road, Evanston, IL 60208, USA

ARTICLE INFO

Article history:
Received 17 February 2009
Received in revised form 22 June 2009
Accepted 26 June 2009
Available online 5 July 2009

Keywords:
Biofouling
Photocatalysis
Ultrafiltration
Titanium dioxide
Biofilm

ABSTRACT

Fouling due to biofilms composed primarily of microorganisms and extracellular polymeric substances is a significant hindrance to membrane filtration in water treatment. The goal of this work was to use a reactive membrane surface to reduce membrane biofouling by coating a ceramic ultrafiltration membrane with the nanoparticulate photocatalyst, TiO_2. 10-Day biofilm growth experiments were conducted to determine the effect of photocatalytic coatings on the formation of a *Pseudomonas putida* biofilm and subsequent changes in membrane flux. Results indicate that a highly hydrophilic, photoreactive coating of mixed phase TiO_2 nanoparticles is effective for the control of biofouling on ceramic ultrafiltration membranes.

1. Introduction

Chemical and biological fouling are major problems in membrane water filtration due to reduced membrane flux, increased energy costs, and system downtime for maintenance [1–3]. Biofouling is the buildup of organic chemicals, microorganisms, and microbial communities at the membrane surface. Biofilms, microbial communities attached to a surface, begin with cell adhesion and progress to thick layers of extracellular polymeric substances, other organic chemicals, and a complex community of microbial cells [4,5] which are difficult to remove.

Recent studies of biofilm formation on membranes identify important bacterial species and critical membrane properties in biofilm initiation. For example, Horsch et al. used fluorescence *in situ* hybridization to characterize biofouling of ultra- and nano-filtration membranes, revealing the importance of gamma-proteobacteria in biofilm colonization when filtering oligotrophic reservoir water [6], and Pasmore et al. studied the effects of various membrane surface properties on the formation of *Pseudomonas aeruginosa* biofilms showing that biofilm initiation is enhanced by rough, hydrophobic, charged surfaces [7]. These insights inform the development of novel membranes to prevent this bacterial adhesion and associated biofouling through a variety of surface modifications to improve hydrophilicity and prevent organic adsorption and bacterial proliferation [8–11].

We and others have shown the effectiveness of titanium dioxide coatings in membrane filtration. The advantage of a photocatalytically reactive TiO_2 membrane is the combination of superhydrophilicity (preventing organic partitioning to the membrane surface, thereby hindering bacterial cell attachment [12,13]), photolysis (cleavage of chemical bonds by specific wavelengths of light [14,15]), and photocatalysis (generation of highly reactive hydroxyl radicals for robust oxidation of organic species [16–18] and microorganisms [19]). Kim et al. applied titanium dioxide nanoparticles to a thin-film composite reverse osmosis membrane and found improvement in membrane permeability after incubation in an *E. coli* solution, compared to uncoated thin-film composite membranes, due to the photo-biocidal effect of the TiO_2 [20]. Choi et al. and Madaeni and Ghaemi have synthesized titania-coated membranes and demonstrated lower rates of flux decline over such membranes [21–23]. Additional studies of photocatalytic membranes, and other methods of integrating photocatalysis and membrane filtration (such as using filtration for the recycle of suspended photocatalysts) are reviewed by Ollis [24].

Our previous work showed that membranes coated with titanium dioxide photocatalysts prevent bacterial attachment, an initial stage in biofilm formation [13]. We studied the attachment of *Pseudomonas putida*, a type of gamma-proteobacteria, to ceramic membranes with and without several different types of titanium dioxide photocatalysts. We found a marked reduction in cell attachment on titania-coated membranes after 3 h in low and high organic solution concentrations, in the dark and under UV illumination.

* Corresponding author at: Department of Civil and Environmental Engineering, Northwestern University, 2145 Sheridan Road, Evanston, IL 60208, USA.
Tel.: +1 847 467 4252; fax: +1 847 491 4011.
E-mail address: k-gray@northwestern.edu (K.A. Gray).

0376-7388/$ – see front matter © 2009 Elsevier B.V. All rights reserved.
doi:10.1016/j.memsci.2009.06.049

Under UV illumination, mixed phase photocatalysts, particularly Degussa P25 TiO_2 (P25), not only inhibited cell attachment, but also achieved cell kill. We hypothesize then, that over longer time intervals these phenomena will reduce biofilm formation and growth, and hence biofouling since dead bacterial cells do not propagate or secrete extracellular polymeric substances.

In this work, we test this hypothesis with long-term biofilm growth experiments, to determine if the attachment results predict the course of biofilm development and flux decline. We coat ceramic membranes with active and inactive titania nanoparticles and measure the biofilm volume and flux decline that develop after 10 days of exposure to a dilute *P. putida* culture under UV illumination. By comparing the performance of the membranes, we are able to separate the individual effects of hydrophilicity, photolysis, and photocatalytic activity at the membrane surface.

2. Materials and methods

2.1. Photocatalytic effects on biofilm volume and flux decline

In a first set of tests to examine the accumulation of biofilm volume and flux decline (Set A), P25 titanium dioxide was applied to the surface of six Sterlitech zirconia ultrafiltration (nominal pore size approximately 0.014 μm) membrane discs using dip-coating and heat treatment, as described previously [13]. Six additional zirconia membrane discs were left uncoated to serve as control samples. P25 is a commercially available mixed-phase photocatalyst produced by high temperature flame hydrolysis. The primary particle size is about 30 nm, but the bulk material is highly heterogeneous in particle size resulting in aggregates as large as 1–2 μm. P25 contains nanoclusters of anatase and rutile crystallites (mixed phase) which, when chemically bound and arranged in a particular morphology, have very high photocatalytic activity [18]. In general, P25 is considered to be the standard of highly active photocatalysts, and we have previously explained that this high activity is associated with charge transfer across and the chemical structure of the solid–solid interface [25–28].

P. putida is a Gram-negative, rod-shaped bacterium. It was chosen as the bacterial model because *P. putida* is commonly present throughout the environment, and readily colonizes biofilms [29,30]. The American Type Culture Collection *P. putida* type strain number 12633 was grown in M9 minimal media at 25 °C, maintained at the exponential growth phase (cell concentration of approximately 10^8 cells/mL) in a 1-L chemostat supplied with 1 L/min sterile air, and 100 rpm stirring. This solution was diluted in sterile phosphate buffered saline (PBS) to bring the solution cell concentration to approximately 10^6 cells/mL, a bacterial cell concentration typical of fresh surface waters [31].

The initial flux of each of the 12 membrane discs in the first set of experiments was measured before biofilm growth by determining the flow rate of deionized water through each membrane at a pressure of 15 in. of mercury. Prior to growing a biofilm on the disc, it was placed in a modified quartz glass Petri dish with inlet and outlet ports, and the assembly was sterilized in an autoclave. Twelve sterile Petri dish assemblies were arranged such that six of the discs were illuminated and the remaining six were covered with aluminum foil to prevent UV light penetration to be used as dark controls. Using sterile tubing and a 12-line peristaltic pump, the dilute *P. putida* culture was pumped across the surface of each of the membrane discs at a rate of 1.15 mL/min. The solution passed once over the discs without recycle. Each day a new batch of dilute cell culture was prepared over the 10-day duration of an experiment using PBS and chemostat effluent. The assembly was illuminated continually for the duration of the test by ultraviolet light from a UVP Blak-Ray Lamp (model B 100 AP) with peak intensity at 365 nm that delivered light with intensity of approximately 5.3 W/m^2 at the membrane surface, as measured by an Apogee spectroradiometer. Samples were tested in triplicate.

After illumination for 10 days, the disc samples were removed from the solution and stained using Invitrogen Molecular Probes Live/Dead stain, containing Syto-9 nucleic acid and propidium iodide to mark attached cells as either having intact (live) or ruptured (dead) cell membranes. Samples were also stained with wheat germ agglutinin Alexa Fluor 647 conjugate for simultaneous visualization of n-acetylglucosamine residues, a component of the extracellular polymeric substance (EPS) matrix [32]. Samples were maintained in PBS at 4 °C for microscopy. Confocal laser scanning microscopy (CLSM) was used to quantify the biofilm at the surface of the membrane samples in terms of bacterial cell volume. Each sample was analyzed in 375 μm × 375 μm sections, collecting a stack of images in 1 μm vertical intervals throughout the thickness of the biomass (typically about 50 images per stack), using an upright Leica confocal microscope, model DM RXE-7 with a 40× dipping lens. Image J software was used to calculate cell (or EPS) volume by determining the total area in each image that had cell matter (a range of 0–140,625 μm^2), multiplying the cell matter area in each image by the 1 μm thickness of the interval, and summing the cell volume for the stack of images to arrive at a total cell volume per sampling site. The biofilm on each of the membranes was analyzed at three locations in this way. CLSM data was also analyzed to evaluate biofilm thickness as well as the maximum percentage of the sampled surface area covered by live cells. We found thickness typically in the 20–90 μm range with some samples up to 160 μm, and live cell coverage ranging up to 74% of the sampled area, but given the three-dimensional heterogeneity inherent to biofilm structure [33], biofilm volume provided a more rigorous basis for comparison. After microscopy, the deionized water flux through each membrane was measured for comparison to the initial flux.

2.2. Photocatalytic effects vs. hydrophilic and photolytic effects on biofilm control

To clarify the roles of hydrophilicity, photolysis, and photocatalysis at the membrane surface, a second set of zirconia membrane discs were prepared using P25 and non-catalytically active rutile, as well as zirconia discs left uncoated (Set B). Illuminated P25 membranes should resist biofilm growth through a combination of mechanisms: hydrophilicity, photolysis, and photocatalysis. The rutile surface allows us to isolate the photocatalytic effect by producing a similar hydrophilic and photolytic environment without photocatalysis. To this end, a nanocrystalline pure-phase rutile powder was synthesized by a low-temperature hydrothermal method using a titanium(IV) chloride precursor, as described by Li et al. [34]. The rutile nanocrystals were rod-shaped with a diameter of about 20 nm and a length of about 150 nm and tended to form micron-sized aggregates, as shown in Fig. 1.

Sessile water drop shape analysis was used to characterize the hydrophobic/hydrophilic nature of the rutile coatings, using a technique described previously [13]. In short, deionized water was dropped onto the surface of glass slides coated with zirconia and titania at a rate of 3 μL/min to form droplets of ~0.5 μL with a Krüss model DSA100 drop shape analyzer. The sessile water drop contact angle was determined using a circle-fitting method. Five measurements were taken on the sample. The rutile coating was found to be as superhydrophilic as the P25 coating [13], both having water drop contact angles below the measurement limit of the test. Zirconia has a contact angle of 5°, indicating it is less hydrophilic.

It is well established that mixed phase P25 is a highly active photocatalyst, while rutile has a much lower reactivity rate, due to high rates of charge recombination [35]. The relatively low

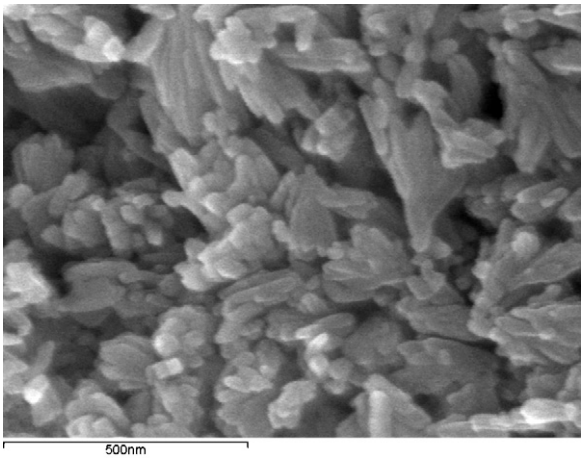

Fig. 1. Electron micrograph of rutile TiO_2. Scale bar 500 nm. Used with permission of Gonghu Li.

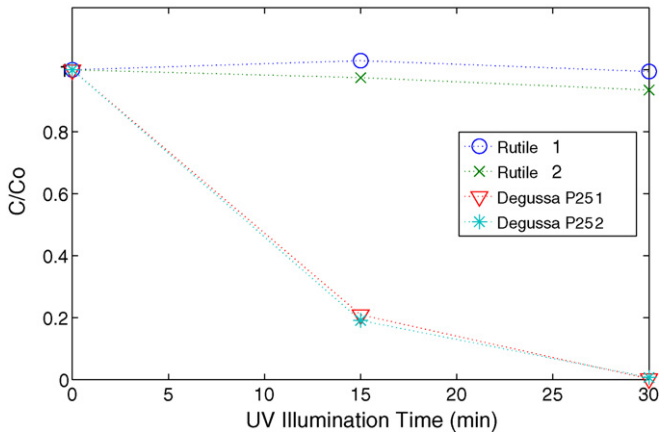

Fig. 2. Comparison of methylene blue degradation by mixed phase P25 and rutile confirms that rutile is essentially photocatalytically inactive.

reactivity of this rutile nanopowder was confirmed by methylene blue degradation. A solution of 30 mL of 0.0125 g/L methylene blue and 2 g/L TiO_2 (either P25 or rutile) was illuminated for 30 min with the 100 W mercury vapor lamp. For each experiment, an aliquot of solution was filtered and immediately analyzed for methylene blue concentration as measured by a Hitachi U-2000 UV–visible spectrophotometer. In an average of two tests, only 3.5% of the methylene blue was degraded by the rutile powder, compared to 99.5% degradation by P25, as shown in Fig. 2.

Biofilm growth experiments were performed under slightly different culture conditions than Set A, using *P. putida* culture in M9 minimal media diluted in 10% PBS solution to achieve the same cell concentration of 10^6 cells/mL. The lower salt concentration (10% PBS in Set B vs. 100% PBS in Set A) resulted in thicker, more mature biofilms after 10 days, consistent with related biofilm studies in varying salt and nutrient levels in solution [36,37]. A summary of test conditions and effects that could be present is shown in Table 1.

3. Results and discussion

A large degree of variability is inherent in biological systems and even small differences in initial growth can be amplified over a relatively long growth period such as the 10-day time interval used for the biofilms studied here. To analyze these data, the heteroscedastic *t*-test, which is used for cases in which sample populations are fewer than 30 and the unknown variances of two populations are not equal, was applied to determine differences between average sample values at a confidence interval of at least 80% [38]. When differences in sample averages are indicated as "significant," the differences have been statistically determined by this metric.

Table 1
Coatings and illumination for samples in experimental sets A and B.

Set	Conditions	Superhydrophilic effect	Photolytic effect	Photocatalytic effect
A, B	Dark zirconia	–	–	–
B	Dark rutile	X	–	–
A, B	Dark P25	X	–	–
A, B	Illuminated zirconia	–	X	–
B	Illuminated rutile	X	X	–
A, B	Illuminated P25	X	X	X

3.1. Photocatalytic effects on biofilm volume and flux decline

The results shown in Fig. 3 illustrate the combined influence of hydrophilicity, UV illumination, and photocatalysis on biofilm growth over the 10-day experiments (Set A). Statistically significant reduction in biofilm volume under the illuminated conditions was observed for the uncoated zirconia membrane in comparison to the dark zirconia system, which can be attributed to photolysis (reaction driven by light energy alone). Statistically significant reduction in biofilm volume was also observed on the P25-coated membranes under dark conditions in comparison to the dark zirconia, and we attribute this to the superhydrophilic nature of the P25 surface. Control of biofilm growth was the greatest in the illuminated P25 systems, which can be explained by the combination of hydrophilic, photolytic, and photocatalytic effects. The average cell volume in illuminated P25 samples was significantly less than the cell volume in other cases: 25% of the illuminated zirconia volume and 3% of the dark zirconia volume.

Analysis of biofilm thickness and surface coverage supports biofilm volume findings. While there were no significant differences observed in biofilm thickness (illuminated P25: 66.5 ± 52.7 μm; dark zirconia: 73.6 ± 42.4 μm), the illuminated P25 samples had the lowest maximum live cell surface coverage of any type (illuminated P25: 0.6 ± 0.8%; dark zirconia: 10.0 ± 10.8%).

As shown in Fig. 4, there was significantly greater n-acetylglucosamine residue volume in the biofilms grown on the dark zirconia membranes as compared to the volume measured in the illuminated samples and the dark P25 samples. These data confirm the trends observed in Fig. 3 and illustrate that over the 10-day biofilm growth experiment, the control of cell attachment

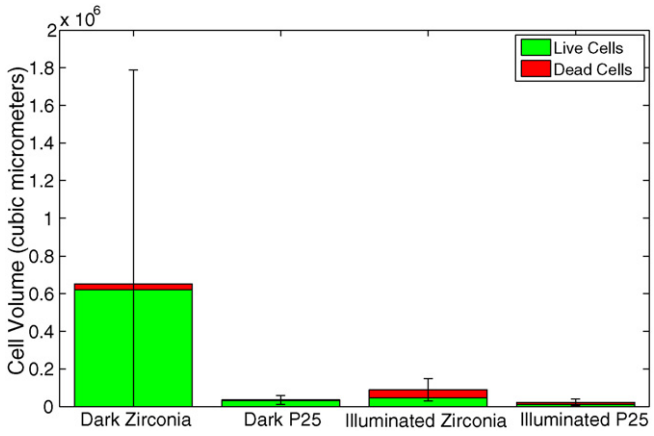

Fig. 3. Comparison of live and dead cell volume in biofilms formed on ceramic membranes after 10 days of exposure to cell culture (each bar is an average of nine readings for three locations on each of three samples).

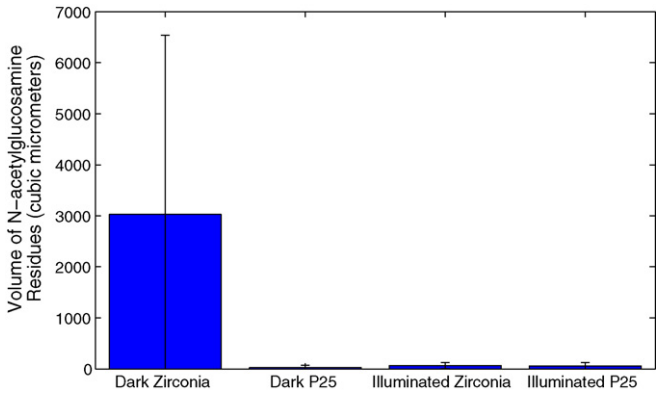

Fig. 4. Comparison of extracellular polymeric substance volume in biofilms formed on ceramic membranes after 10 days, as measured by n-acetylglucosamine residues (each bar is an average of three samples).

and growth also results in significantly diminished extracellular polymer substance production by hydrophilic, photolytic, and photocatalytic effects.

The average flux decline for each sample type is shown in Fig. 5. Statistical comparison of these data indicates that the flux decline for zirconia membranes was significantly different from flux decline for P25 membranes, but that there was no statistically significant difference between illuminated and dark P25 samples and no statistically significant difference between illuminated and dark zirconia samples.

The high level of flux decline for the illuminated zirconia samples, which had relatively little biofilm cell volume (Figs. 3 and 4), is puzzling at first glance. To make sense of these data, it is important to note the difference in pore size caused by the addition of the photocatalyst. Photocatalyst dip-coating reduced the average membrane pore size by nearly one order of magnitude, from 0.8 to 0.1 μm as measured by deionized water flux at 15 in. of mercury transmembrane pressure. This creates a difference in initial water flux, with approximately one half the flux through the coated membranes in comparison to the uncoated zirconia membranes (see Table 2 for water flux values). Flux decline is presented as a fraction of initial flux in Fig. 5. The larger pore size of the uncoated membranes is more susceptible to clogging by the *P. putida* bacterial cells (typically 0.5–1 μm in diameter) within the pores where photolysis becomes less effective, in contrast to the 0.1 μm pores of the titania membranes which would exclude these bacterial cells, retaining them near the surface [39]. EPS may also be more likely to coat the membrane pores of less-hydrophilic zirconia membranes, as

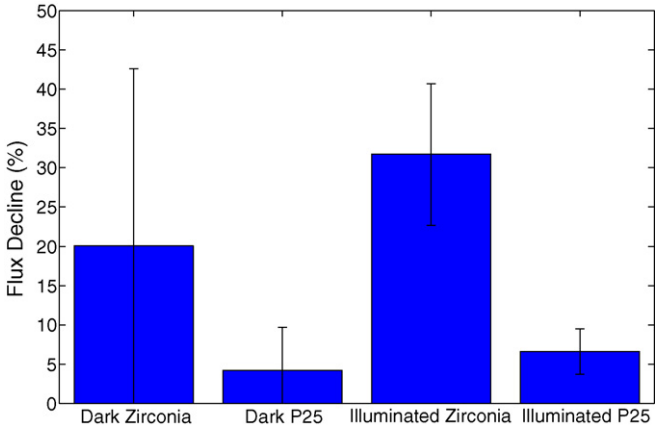

Fig. 5. Average flux decline over membranes after 10 days of biofilm growth.

Table 2
Flux values for membranes before and after fouling.

Sample	Pre-test flux (mL/h)	Post-test flux (mL/h)
Dark zirconia	1015	610
Dark zirconia	1246	938
Dark zirconia	1112	1160
Dark P25	512	510
Dark P25	590	580
Dark P25	620	555
Illuminated zirconia	1272	780
Illuminated zirconia	1627	1060
Illuminated zirconia	1310	1028
Illuminated P25	540	511
Illuminated P25	594	535
Illuminated P25	461	440

compared to superhydrophilic titania membranes. While the pore sizes are different between these zirconia and P25 samples, this is a parameter that can be tuned in the application of this technology.

3.2. Photocatalytic effects vs. hydrophilic and photolytic effects on biofilm control

The results of the experiments presented above (Set A) do not provide information about the individual extent of the hydrophilic, photolytic, and photocatalytic effects. Therefore, we conducted an additional set of experiments (Set B) in order to separate the relative contributions of these effects on biofilm control in this system. (The term 'significantly different' here continues to refer to differences that are statistically significant at a confidence interval of at least 80% by the heteroscedastic *t*-test.) As shown in Fig. 6, superhydrophilic dark rutile and dark P25 samples do not differ statistically from hydrophilic dark zirconia samples, illustrating that the superhydrophilic effect due to P25 (Fig. 3) is limited to conditions in which less dense biofilms form (such as in Fig. 3). When denser, more mature biofilms are allowed to form (Fig. 6), the hydrophilic effect no longer exerts a controlling influence. The illuminated zirconia samples have significantly less cell volume than the dark zirconia samples (Fig. 6), revealing the photolytic effect in controlling biofilm growth. The average cell volume for the illuminated rutile samples, however, is not significantly different from the average cell volume for the dark zirconia samples, which indicates that there is a limit to the photolytic efficacy in controlling biofilm growth. Although the identical illumination conditions were used for the illuminated zirconia and rutile membranes, we attribute

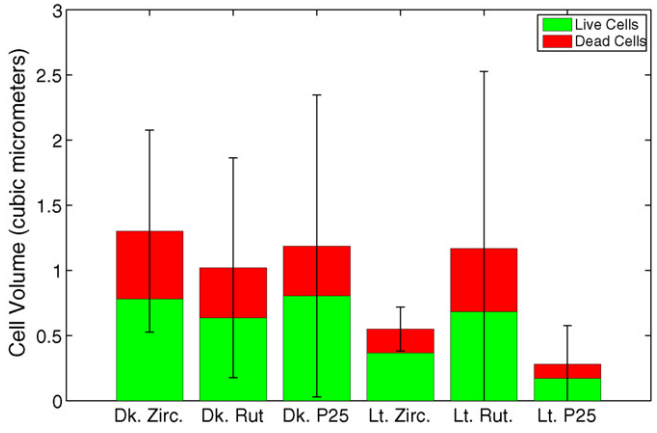

Fig. 6. Comparison of live and dead cell volume in biofilms for reactive P25 membranes and zirconia (Zirc.) and rutile (Rut.) control membranes. "Dk." indicates dark conditions; "Lt." indicates ultraviolet light illumination conditions.

the variability in these data to that which is inherent in biological systems. Despite this experimental variability, these results clearly show the superior function of photocatalysis on the illuminated P25 samples, which have significantly less cell volume than both types of illuminated non-catalytic samples.

The illuminated P25 samples statistically have the lowest average cell volume with significantly less biofilm growth than all other samples. These results indicate that even though hydrophilic and photolytic effects are important for controlling biofilm growth at early stages of biofouling (Fig. 3), the photocatalytic effect is more robust. In denser biofilms (Fig. 6), the hydrophilic and photolytic effects were ultimately overwhelmed, while the photocatalytic P25 membranes showed superior biofilm control.

Analysis of biofilm thickness and surface coverage supports biofilm volume findings. While there were no significant differences observed in biofilm thickness (illuminated P25: $52.4 \pm 18.9\ \mu m$; dark zirconia: $54.7 \pm 17.9\ \mu m$), the illuminated P25 samples had the lowest maximum live cell surface coverage of any type (illuminated P25: $9.7 \pm 7.2\%$; dark zirconia: $36.2 \pm 18.0\%$).

4. Conclusions

These results show that the reduced bacterial cell attachment and increased cell kill on the photocatalytic membranes in our previous work can be extended to the long-term control of biofilm formation and flux decline. We show that photocatalytic mixed phase TiO_2 coatings such as P25 control the growth of biofilms and lessen the flux decline on ceramic ultrafiltration membranes during a 10-day growth period. Hydrophilic and photolytic effects are important in preventing biofilm growth, but membranes coated with P25 photocatalyst show superior biofouling resistance compared to uncoated zirconia membranes and membranes coated with hydrophilic, non-reactive rutile titanium dioxide, even when all of these are illuminated with UV light. These results are consistent with other work in the area of TiO_2-enhanced membranes and films, which have been shown to reduce chemical fouling, inactivate microorganisms, and reduce bacterial cell adhesion. This study differs from previous work by focusing on the growth of biofilms over an extended period of time. Compared to alternative methods of preventing biofouling, which rely predominantly on hydrophilicity alone, the use of titanium dioxide adds a photoreactive element to biofouling resistance, actively killing bacteria and oxidizing organic chemicals, which is necessary for robust biofilm control.

Acknowledgements

This work was supported by the National Science Foundation under Grant No. 0403581. Thanks to the Evonik Degussa Corporation for their donation of P25. The confocal microscopy work was performed in the Biological Imaging Facility on the Evanston campus of Northwestern University. Thanks to William Russin, Gonghu Li, Yuan Yao, Rebecca Penskar, Andrew Reiter, Virginia Palmer, Daniel Paschall, Charlette Broxton, and Samantha Hilson for their experimental assistance.

References

[1] M.F.A. Goosen, S.S. Sablani, H. Ai-Hinai, S. Ai-Obeidani, R. Al-Belushi, D. Jackson, Fouling of reverse osmosis and ultrafiltration membranes: a critical review, Separation Science and Technology 39 (2004) 2261–2297.
[2] E.M. Gwon, M.J. Yu, H.K. Oh, Y.H. Ylee, Fouling characteristics of NF and RO operated for removal of dissolved matter from groundwater, Water Research 37 (2003) 2989–2997.
[3] B. Van der Bruggen, C. Vandecasteele, T. Van Gestel, W. Doyen, R. Leysen, A review of pressure-driven membrane processes in wastewater treatment and drinking water production, Environmental Progress 22 (2003) 46–56.
[4] W.M. Dunne, Bacterial adhesion: seen any good biofilms lately? Clinical Microbiology Reviews 15 (2002) 155–166.
[5] J.W. Costerton, Z. Lewandowski, D.E. Caldwell, D.R. Korber, H.M. Lappinscott, Microbial biofilms, Annual Review of Microbiology 49 (1995) 711–745.
[6] P. Horsch, A. Gorenflo, C. Fuder, A. Deleage, F.H. Frimmel, Biofouling of ultra- and nanofiltration membranes for drinking water treatment characterized by fluorescence *in situ* hybridization (FISH), Desalination 172 (2005) 41–52.
[7] M. Pasmore, P. Todd, S. Smith, D. Baker, J. Silverstein, D. Coons, C.N. Bowman, Effects of ultrafiltration membrane surface properties on *Pseudomonas aeruginosa* biofilm initiation for the purpose of reducing biofouling, Journal of Membrane Science 194 (2001) 15–32.
[8] Y.Q. Wang, Y.L. Su, Q. Sun, X.L. Ma, Z.Y. Jiang, Generation of anti-biofouling ultrafiltration membrane surface by blending novel branched amphiphilic polymers with polyethersulfone, Journal of Membrane Science 286 (2006) 228–236.
[9] J. Hyun, H. Jang, K. Kim, K. Na, T. Tak, Restriction of biofouling in membrane filtration using a brush-like polymer containing oligoethylene glycol side chains, Journal of Membrane Science 282 (2006) 52–59.
[10] J. Pieracci, J.V. Crivello, G. Belfort, Photochemical modification of 10 kDa polyethersulfone ultrafiltration membranes for reduction of biofouling, Journal of Membrane Science 156 (1999) 223–240.
[11] N. Hilal, L. Al-Khatib, B.P. Atkin, V. Kochkodan, N. Potapchenko, Photochemical modification of membrane surfaces for (bio)fouling reduction: a nano-scale study using AFM, Desalination 158 (2003) 65–72.
[12] N. Sakai, A. Fujishima, T. Watanabe, K. Hashimoto, Quantitative evaluation of the photoinduced hydrophilic conversion properties of TiO_2 thin film surfaces by the reciprocal of contact angle, Journal of Physical Chemistry B 107 (2003) 1028–1035.
[13] S. Ciston, R.M. Lueptow, K.A. Gray, Bacterial attachment on reactive ceramic ultrafiltration membranes, Journal of Membrane Science 320 (2008) 101–107.
[14] R. Andreozzi, M. Raffaele, P. Nicklas, Pharmaceuticals in STP effluents and their solar photodegradation in aquatic environment, Chemosphere 50 (2003) 1319–1330.
[15] E.M. Espeland, R.G. Wetzel, Complexation, stabilization, and UV photolysis of extracellular and surface-bound glucosidase and alkaline phosphatase: implications for biofilm microbiota, Microbial Ecology 42 (2001) 572–585.
[16] E.P. Reddy, B. Sun, P.G. Smirniotis, Transition metal modified TiO_2-loaded MCM-41 catalysts for visible- and UV-light driven photodegradation of aqueous organic pollutants, Journal of Physical Chemistry B 108 (2004) 17198–17205.
[17] K. Hashimoto, H. Irie, A. Fujishima, TiO_2 photocatalysis: a historical overview and future prospects, Japanese Journal of Applied Physics Part 1-Regular Papers Brief Communications and Review Papers 44 (2005) 8269–8285.
[18] M.R. Hoffmann, S.T. Martin, W.Y. Choi, D.W. Bahnemann, Environmental applications of semiconductor photocatalysis, Chemical Reviews 95 (1995) 69–96.
[19] K. Sunada, T. Watanabe, K. Hashimoto, Studies on photokilling of bacteria on TiO_2 thin film, Journal of Photochemistry and Photobiology A: Chemistry 156 (2003) 227–233.
[20] S.H. Kim, S.Y. Kwak, B.H. Sohn, T.H. Park, Design of TiO_2 nanoparticle self-assembled aromatic polyamide thin-film-composite (TFC) membrane as an approach to solve biofouling problem, Journal of Membrane Science 211 (2003) 157–165.
[21] H. Choi, E. Stathatos, D.D. Dionysiou, Photocatalytic TiO_2 films and membranes for the development of efficient wastewater treatment and reuse systems, Desalination 202 (2007) 199–206.
[22] S.S. Madaeni, N. Ghaemi, Characterization of self-cleaning RO membranes coated with TiO_2 particles under UV irradiation, Journal of Membrane Science 303 (2007) 221–233.
[23] H. Choi, A.C. Sofranko, D.D. Dionysiou, Nanocrystalline TiO_2 photocatalytic membranes with a hierarchical mesoporous multilayer structure: synthesis, characterization, and multifunction, Advanced Functional Materials 16 (2006) 1067–1074.
[24] D.F. Ollis, Integrating photocatalysis and membrane technologies for water treatment, Advanced Membrane Technology (2003) 65–84.
[25] D.C. Hurum, A.G. Agrios, K.A. Gray, T. Rajh, M.C. Thurnauer, Explaining the enhanced photocatalytic activity of Degussa P25 mixed-phase TiO_2 using EPR, Journal of Physical Chemistry B 107 (2003) 4545–4549.
[26] G.H. Li, L. Chen, M.E. Graham, K.A. Gray, A comparison of mixed phase titania photocatalysts prepared by physical and chemical methods: the importance of the solid–solid interface, Journal of Molecular Catalysis A: Chemical 275 (2007) 30–35.
[27] D.C. Hurum, K.A. Gray, T. Rajh, M.C. Thurnauer, Recombination pathways in the Degussa P25 formulation of TiO_2: surface versus lattice mechanisms, Journal of Physical Chemistry B 109 (2005) 977–980.
[28] G.H. Li, K.A. Gray, The solid–solid interface: explaining the high and unique photocatalytic reactivity of TiO_2-based nanocomposite materials, Chemical Physics 339 (2007) 173–187.
[29] K.N. Timmis, *Pseudomonas putida*: a cosmopolitan opportunist par excellence, Environmental Microbiology 4 (2002) 779–781.
[30] T. Tolker-Nielsen, U.C. Brinch, P.C. Ragas, J.B. Andersen, C.S. Jacobsen, S. Molin, Development and dynamics of Pseudomonas sp biofilms, Journal of Bacteriology 182 (2000) 6482–6489.
[31] D. Scavia, G.A. Laird, G.L. Fahnenstiel, Production of Planktonic bacteria near Lake-Michigan, Limnology and Oceanography 31 (1986) 612–626.
[32] S.C. Kachlany, S.B. Levery, J.S. Kim, B.L. Reuhs, L.W. Lion, W.C. Ghiorse, Structure and carbohydrate analysis of the exopolysaccharide capsule of *Pseudomonas putida* G7, Environmental Microbiology 3 (2001) 774–784.
[33] D. Debeer, P. Stoodley, F. Roe, Z. Lewandowski, Effects of biofilm structures on oxygen distribution and mass-transport, Biotechnology and Bioengineering 43 (1994) 1131–1138.

[34] G. Li, N. Dimitrijevic, L. Chen, T. Rajh, K.A. Gray, Role of surface/interfacial Cu^{2+} sites in the photocatalytic activity of coupled CuO–TiO_2 nanocomposites, Journal of Physical Chemistry C 112 (2008) 19040–19044.
[35] A. Furube, T. Asahi, H. Masuhara, H. Yamashita, M. Anpo, Charge carrier dynamics of standard TiO_2 catalysts revealed by femtosecond diffuse reflectance spectroscopy, Journal of Physical Chemistry B 103 (1999) 3120–3127.
[36] G.A. O'Toole, R. Kolter, Initiation of biofilm formation in *Pseudomonas fluorescens* WCS365 proceeds via multiple, convergent signalling pathways: a genetic analysis, Molecular Microbiology 28 (1998) 449–461.
[37] X.X. Sheng, Y.P. Ting, S.O. Pehkonen, The influence of ionic strength, nutrients and pH on bacterial adhesion to metals, Journal of Colloid and Interface Science 321 (2008) 256–264.
[38] D.C. Montgomery, G.C. Runger, Applied Statistics and Probability for Engineers, Wiley, Hoboken, NJ, 2007.
[39] G. Hwang, Y.M. Ban, C.H. Lee, C.H. Chung, I.S. Ahn, Adhesion of *Pseudomonas putida* NCIB 9816-4 to a naphthalene-contaminated soil, Colloids and Surfaces B: Biointerfaces 62 (2008) 91–96.